Int. J. Electrochem. Sci., 14 **(2019)** 1163 – 1177, doi: 10.20964/2019.02.40

International Journal of
ELECTROCHEMICAL
SCIENCE
www.electrochemsci.org

Corrosion and Surface Electrochemical Behaviors of Aluminum Alloy 2A12-T3 During Long-Term Exposure at Dry-Hot Climate of Turpan (China)

Ni Li, Chen Man, Junjun Wei, Jizheng Yao, Chaofang Dong[*]

Beijing Advanced Innovation Center for Materials Genome Engineering, Key Laboratory for Corrosion and Protection (MOE), Institute for Advanced Materials and Technology, University of Science and Technology Beijing, Beijing 100083, PR China
[*]E-mail: cfdong@ustb.edu.cn

Received: 3 November 2018 / *Accepted:* 4 December 2018 / *Published:* 5 January 2019

The long-term atmospheric corrosion behaviors of aluminum alloy 2A12-T3 specimens that are exposed in a dry-hot environment for 3 years were investigated via weight loss measurement, electrochemical impedance spectrum (EIS) analysis and several surface analytical techniques. The results demonstrated that the thicknesses of corrosion products that were exposed for 1, 2, and 3 years in Turpan were respectively 2.01 µm, 4.99 µm and 7.97 µm. The average corrosion rate of the 2A12-T3 alloy after exposure for 1, 2 and 3 years were 0.62 $g \cdot m^{-2} \cdot a^{-1}$, 0.42 $g \cdot m^{-2} \cdot a^{-1}$ and 0.34 $g \cdot m^{-2} \cdot a^{-1}$. With the exposure time extending, the corrosion rate decreased owing to the corrosion products covered on the surfaces. According to the electrochemical measurements, the oxide layer primarily influenced the anodic dissolution process. The corrosion types of the 2A12-T3 alloy are pitting and intergranular corrosion in this environment. The dominate corrosion products were Al_2O_3, bayerite ($Al(OH)_3$), boehmite (AlOOH) and $AlCl_3$.

Keywords: dry-hot environment; atmospheric corrosion; pitting; intergranular corrosion; 2A12-T3 alloy.

1. INTRODUCTION

Aluminum alloys of the type 2xxx (Al-Cu-Mg) have been widely used in aerospace industries due to their low density and high strength [1]. Various alloying elements such as Mg, Cu and Fe were added into the Al matrix to realize an excellent combination of strength and ductility [2]. However, the intermetallic particles, which precipitated if the concentration of alloying elements reached a threshold level, had a negative effect on the corrosion resistance of Al alloys [3-5]. As served in the outdoor atmosphere, 2xxx aluminum alloys typically suffered from localized corrosion such as pitting, intergranular corrosion and exfoliation corrosion.

Field exposure testing is the most reliable method for estimating the corrosion performance in actual service environments [6-8]. In the past decades, the field exposure tests of aluminum and its alloys were performed under various atmospheric conditions all over the world [9-12]. Many researchers focused on the studies of atmospheric corrosion in outdoor environments that have high pollutant (mainly Cl^- and SO^{2-}) and relative humidity. Sun et al. [13] studied the atmospheric corrosion behavior of the AA2024 and AA7075 alloy that were exposed in urban, coastal and industrial atmospheres for 20 years. Weight losses for both the AA2024 alloy and the AA7075 alloy increased in the following order (from low to high): urban atmosphere < coastal atmosphere < industrial atmosphere. B. B. Wang [14] investigated the atmospheric corrosion of the 2024-T3 alloy in a salt lake environment in western China, and proposed that a high concentration of Cl^- resulted in a higher corrosion rate in this environment compared to an industrial atmosphere. According to a comparison of the corrosion behaviors of the aluminum alloys in various atmospheric environments, the corrosion rate of aluminum alloy is closely related to environmental factors. The dry tropical desert environment, which is a typical climates, is characterized by the low relative humidity and large diurnal temperature variation. This should result in exhibiting the corrosion behaviors in this atmosphere that differ significantly with those in the urban, coastal and industrial environments. However, the corrosion behaviors of aluminum alloys has not been studied to date. The corrosion mechanism of aluminum alloy in the dry tropical desert environment and the influence of the large diurnal temperature variation have not been thoroughly elucidated to date.

In this study, the atmospheric corrosion behaviors of the 2A12-T3 alloy in a dry tropical desert environment after exposure for 1-3 years were studied via field exposure tests. The corrosion kinetic was calculated from the mass loss. To identify the corrosion mechanism of the 2A12-T3 alloy in this environment, the composition and morphology of the corrosion product were analyzed via scanning electron microscopy (SEM), energy dispersive spectrometry (EDS), X-ray diffraction (XRD) and X-ray photoelectron spectroscopy (XPS). The Volta potential of the precipitation was characterized by the scanning kelvin probe force microscopy (SKPFM) to explore the pitting mechanism of the 2A12-T3 alloy.

2. EXPERIMENTAL

2.1. Materials preparation and exposure test

The investigated material was 2A12-T2 aluminum alloy with the chemical composition (wt. %) Al-4.68Cu-1.6Mg-0.53Mn-0.35Fe, as listed in Table 1. Samples with the size of 150mm×75mm×0.9mm were cut from the 2A12-T2 sheet. As shown in Fig. 1, there were many of Al_2CuMg intermetallic particles in the 2A12-T3 alloy. Prior to field exposure, the test samples were mechanically ground by hand using 800 grit SiC grinding papers, degreased in acetone, cleared with distilled water, dehydrated using absolute ethyl alcohol, and then kept in a desiccator for at least 24h. After these treatments, the specimens were weighed on an analytical balance after drying which had an accuracy of 0.1 mg.

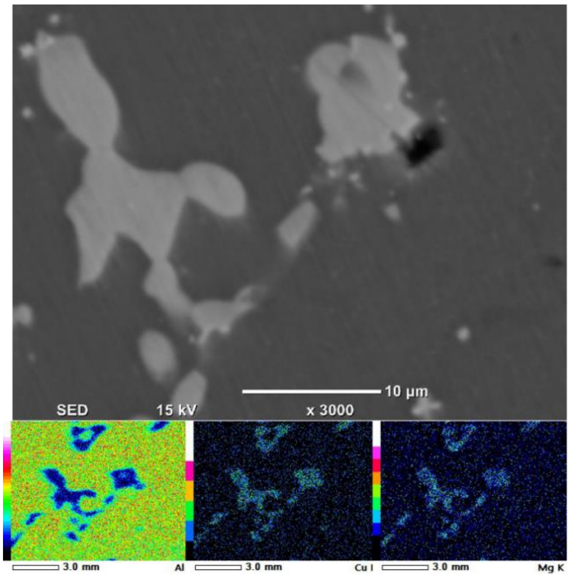

Figure 1. Backscattered electron image of the mechanically polished surface of the 2A12-T3 alloy.

Table 1. Chemical compositions of alloy the 2A12-T3 alloy (wt. %)

Alloy	Fe	Cu	Mg	Mn	Zn	Si	Ti	Al
2A12-T3	0.35	4.68	1.6	0.53	0.10	0.13	0.023	Bal.

2.2. Climatic characteristics of the test site

The samples were exposed in Turpan, which belonged to a dry tropical desert environment that has a wide diurnal temperature variation, long sunshine time, low rainfall and high evaporation. The soil in Turpan was saline and alkaline. The annual wind speed was 2.5 m/s, and there were frequent sandstorms. The meteorological parameters in Turpan were listed in Table 2. The average annual rainfalls for the previous 3 years were only 1.2, 9.7 and 7.8 mm. The relative humidity was high in November, December and January every year. Over this period, the temperature was relative low. Moreover, according to Fig. 2 showed that the diurnal temperature variation could reach up to 12℃ in Turpan, which led to the formation of water droplets.

Table 2. Meteorological data of the Turpan exposure station (2012-07~2015-06)

Data	2012						2013					
	7	8	9	10	11	12	1	2	3	4	5	6
Average temperature /℃	35.8	33.8	27.1	16.3	1.6	-6.7	-12.6	1.5	16.4	23.0	28.9	33.2
Average highest temperature /℃	39.8	39.2	32.8	25.2	6.2	-2.6	-7.2	6.0	20.6	27.0	32.0	37.7

Average lowest temperature /°C	30.4	28.4	21.5	11.2	-2.1	-9.9	-16.4	-2.9	7.7	14.1	20.9	28.6
Average relative humidity / %	21	14	20	26	30.1	59.3	80.0	42.8	17.4	15.1	14.1	18.3
Average wind speed / m·s^{-1}	3.4	3.7	2.2	2.4	2.5	1.5	1.0	2.0	2.1	2.6	3.3	4.1

Data	2013						2014					
	7	8	9	10	11	12	1	2	3	4	5	6
Average temperature /°C	35.1	34.6	26.7	19.3	5.0	-3.2	-7.0	-0.2	12.9	20.8	27.1	31.9
Average highest temperature /°C	39.9	41.3	26.8	19.5	9.9	2.1	0.9	5.0	18.1	26.3	33.3	37.5
Average lowest temperature /°C	28.9	30	26.5	19.2	0.7	-5.9	-11.4	-5.1	7.1	14.8	20.4	26.3
Average relative humidity / %	19.1	17.7	18.6	23.4	43.0	58.0	49.7	27.9	18.0	17.0	17.0	21
Average wind speed / m·s^{-1}	3.5	3.21	2.75	2.20	1.80	1.60	1.60	2.10	2.1	2.40	3.20	3.3

Data	2014						2015					
	7	8	9	10	11	12	1	2	3	4	5	6
Average temperature /°C	35.1	34.3	27.0	18.9	5.8	-3.1	-7.1	-0.1	12.0	20.2	27.1	35.0
Average highest temperature /°C	40.3	44.03	42.8	34.8	22.2	6.0	-1.6	5.34	18.2	26.4	33.6	40.9
Average lowest temperature /°C	29.5	23.0	16.0	14.8	-5.2	-13.6	-11.6	-5.1	5.9	14.1	20.3	29.5
Average relative humidity / %	20.0	16.1	20.0	24	21.8	57.9	49.7	27.9	17.4	17.2	17.1	19.1
Average wind speed / m·s^{-1}	3.3	3.03	2.65	2.20	2.30	1.60	1.60	2.12	2.37	2.79	3.16	3.21

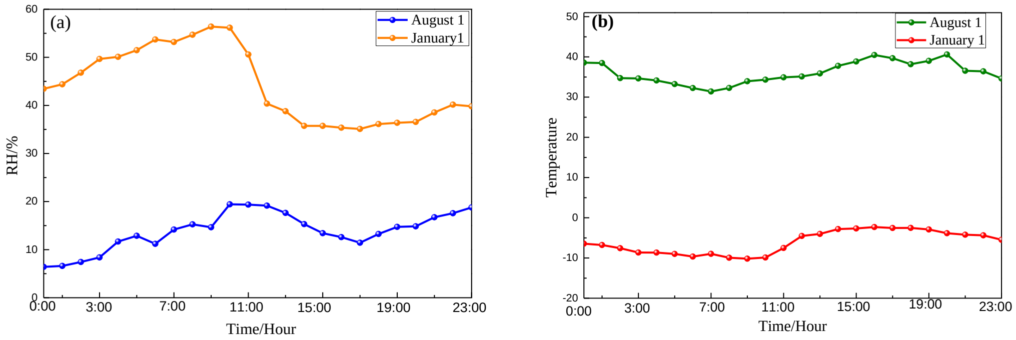

Figure 2. Average relative humidity and average temperature on August 1, and January 1, 2014; (a) average relative humidity and (b) average temperature.

2.3. Weight loss measurement

The corrosion products were chemically eliminated by immersing the specimens in a solution (50 ml H_3PO_4 + 20 g CrO_3 + 1 L H_2O) at 80°C for 8 min, and then washed with lots of distilled water. According to the previous literature [16], the corrosion rate was calculated via Equation (1).

$$v_1 = (w_0 - w_1)/(S * t) \qquad (1)$$

where v_1 is the corrosion rate ($g \cdot m^{-2} \cdot a^{-1}$), w_0 and w_1 are the original and the final weights (g), S is the surface area (m^{-2}), and t is the exposure time (year).

2.4 Morphology observation and composition analysis

The macroscopic morphology of the sample was observed using a digital camera. The micromorphology of the surface and a cross-section of the 2A12-T3 alloy were identified by using a scanning electron microscope (SEM; FEI Quanta250) that was equipped with an energy dispersive spectrometer (EDS) and could generate backscattered electron Kikuchi patterns (BEKPs) for combined chemical and structural phase identification. The compositions of the corrosion products were determined via X-ray photoelectron spectroscopy (XPS) and X-ray diffraction (XRD).

2.5 Electrochemical impedance spectroscopy

Electrochemical impedance spectroscopy (EIS) measurements were conducted using a PARSTAT 2273 work-station and a conventional three-electrode electrochemical cell was used in 0.1wt% Na_2SO_4 solution at ambient temperature. EIS tests were performed by applying a sinusoidal perturbation with a 10 mV (vs SCE) of amplitude (rms) in the frequency range of 0.01-10^5 Hz. The ZSimpWin 3.3 software was utilized to fit the data.

2.6 Scanning kelvin probe force microscopy

The SKPFM measurements were obtained via an atomic force microscopy (Multimode VIII, Bruker). To map the surface potential, SKPFM was performed using a PFQNE-AL probe with a silicon tip on a silicon nitride cantilever. The topography of the sample surface was obtained during the first pass. In the second pass, the cantilever was lifted to an appropriate height to prevent the topographic features from influencing the mapping of the potential. All of the images in this work were obtained at a scanning rate of 0.45 Hz with a resolution of 512 × 512, and the intermetallic particles were identified with the help of a Vickers particle counter.

3. RESULTS AND DISCUSSION

3.1 Weight loss

The weight loss and corrosion rate of the 2A12-T3 alloy that was exposed at the Turpan test site for 1-3 years are plotted in Fig. 3. The average corrosion rate (g·m^{-2}·a^{-1}) which was calculated via using Equation (1), exhibits a decreasing trend over the exposure periods. This finding is attributed to the protection of corrosion products that cover on the surfaces. In the dry tropical desert environment, the corrosion rate of the specimens that were exposed in Turpan for 1-3 years were respectively 0.62 g·m^{-2}·a^{-1}, 0.418 g·m^{-2}·a^{-1} and 0.335 g·m^{-2}·a^{-1}, respectively, which were considerably smaller than the corrosion rates of the 2024 alloy that was exposed to coastal and industrial environments (4.293 g·m^{-2}·a^{-1} and 2.766 g·m^{-2}·a^{-1}) [15]. This finding is attributed to the low relative humidity at the exposure site.

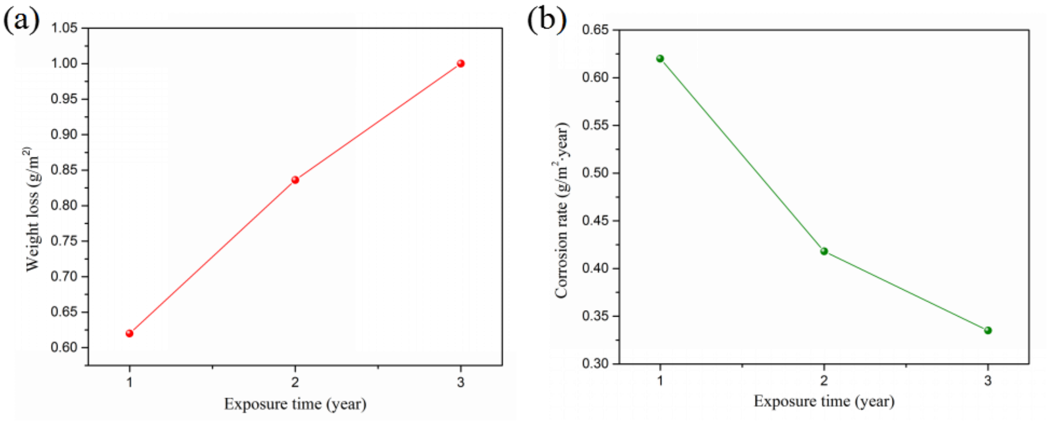

Figure 3. Weight loss and average corrosion rate of the 2A12-T3 alloy during exposure in a dry and tropical desert atmosphere for 3 years.

Several studies [16-17] have demonstrated that the corrosion rate of an aluminum alloy after long-term exposure for a long time can be expressed as:

$$C = At^n \qquad (2)$$

where A and C are the corrosion losses after exposure for one and *t* years and *n* is a constant that represents the propensity for corrosion. Table 3 lists the fitting results of the constants (A, n and R^2), which demonstrate that the relationship between t and C obeys the power function.

Table 3. Corrosion kinetic coefficients for 2A12-T3 in Turpan

	A	n	R^2
2A12-T3	0.618	0.442	0.999

3.2 Morphology observation

Fig. 4 presents the optical views of the macroscopic morphology of the 2A12-T3 alloy specimens that were exposed in Turpan for 1-3 years. Localized corrosion was observed on the surfaces of the specimens. The views of the front face and back face showed that the specimens lost brightness and became rough with a yellowish gray patina. After removing the corrosion products of the specimens, the types of the corrosion on the 2A12-T3 alloy surface were identified as pitting and intergranular corrosion as shown in Fig. 5. With the increase of the exposure time, the number and size of the pits increased gradually. The localized corrosion that occurred on the front face was much more serious than on the back face.

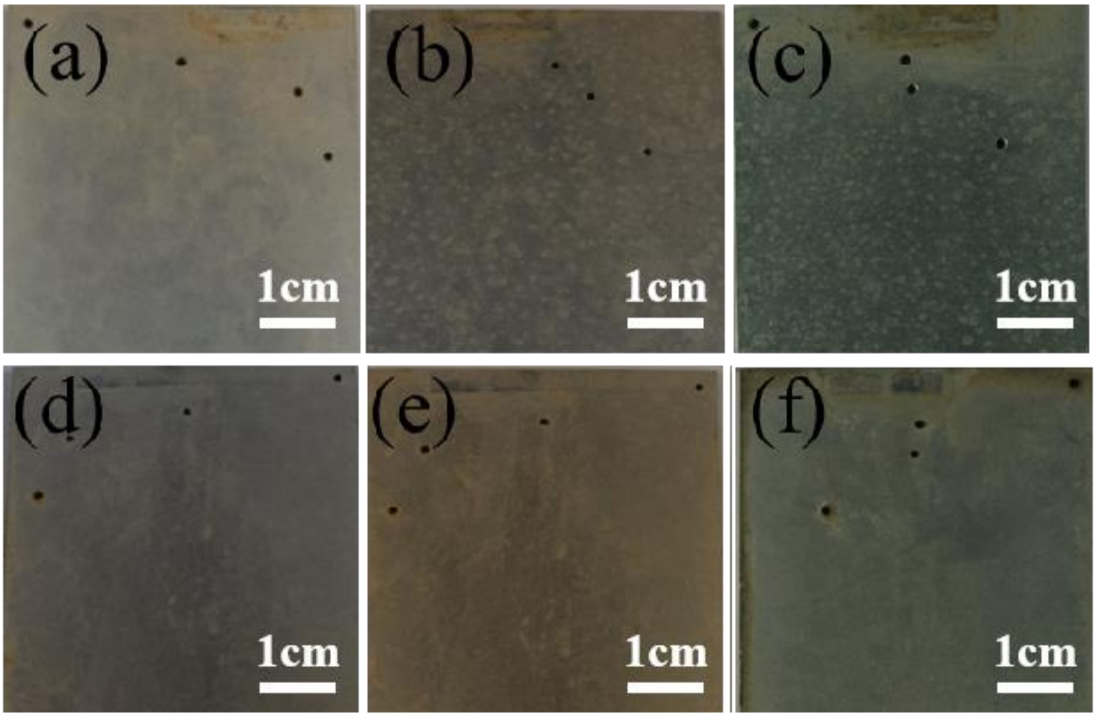

Figure 4. Macromorphology of 2A12-T3 alloy specimens exposed in Turpan for different time: (a) 1 year back face, (b) 2 years back face, (c) 3 years back face, (d) 1 year front face, (e) 2 years front face, (f) 3 years front face.

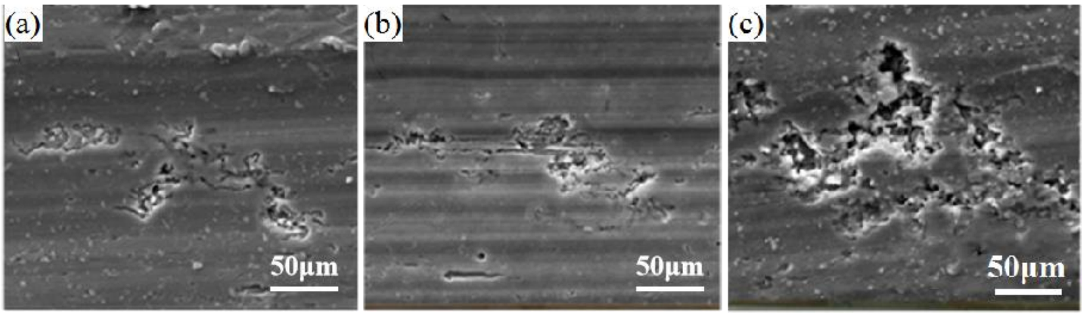

Figure 5. SEM images of 2A12-T3 alloy exposed in Turpan for different time after removing the corrosion products: (a) 1 year, (b) 2 years and (c) 3 years.

The cross-sectional morphologies of the 2A12-T3 alloy specimens after exposure in Turpan for 1-3 years were analyzed via SEM in Fig. 6. After exposure for 1 and 2 years, the corrosion products were compact and continuous. After exposure in Turpan for 3 years, the corrosion products layer and aluminum alloy substrate became stratified. The average cladding thicknesses after exposure for 1, 2 and

3 years were respectively 2.01 µm, 4.99 µm and 7.97 µm, respectively. The corrosion products layer that were exposed in Turpan were much thinner than that were reported in the literature after the surfaces of the aluminum alloy was exposed to a marine atmospheric environment (10-30 um) [17]. During exposure at a dry-hot site, a large ohmic potential drop in the thin water layer on the surface of the sample would decrease the likelihood of galvanic coupling of alloy constituents.

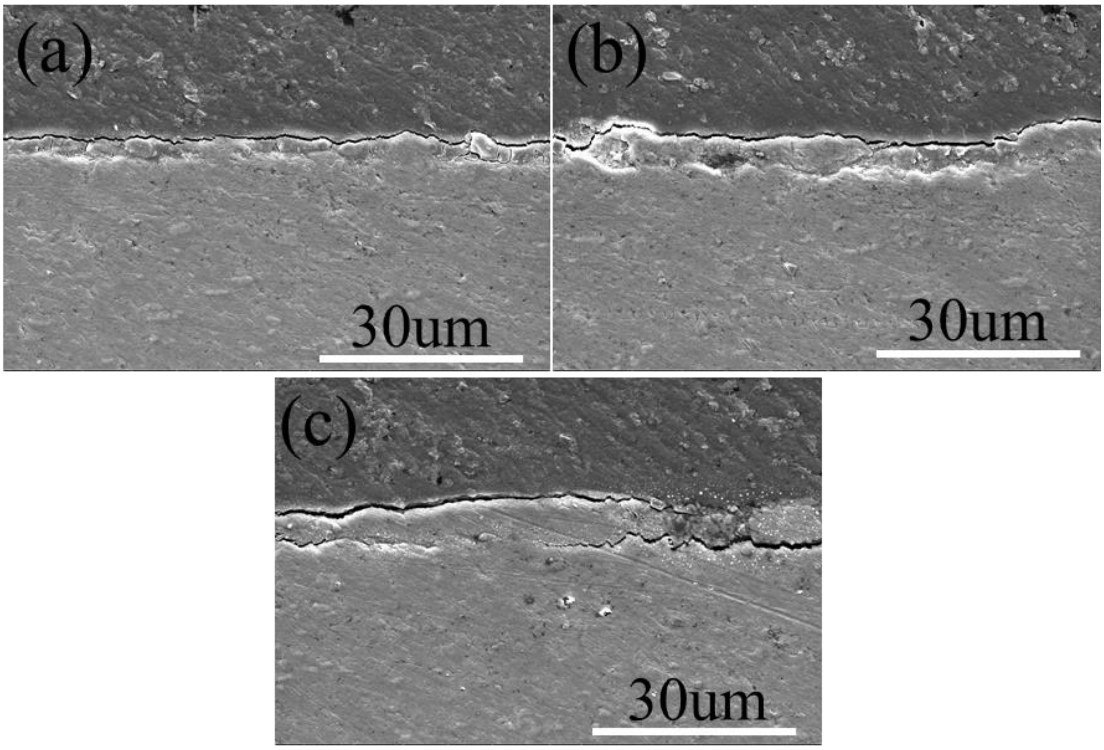

Figure 6. Cross-sectional morphology of 2A12-T3 alloy specimens that were exposed for various lengths of time: (a) 1 year; (b) 2 years; (c) 3 years.

3.3 Corrosion products analysis

The SEM images of the corrosion products that formed on the 2A12-T3 alloy after exposure for 1-3 years were shown in Fig. 7. The chemical compositions of the corrosion products were determined via EDS analysis. There are many deposits on the surface that adhere to the substrate. The corrosion products that formed on the 2A12-T3 alloy consisted of a dark-gray compact layer and a loose white surface layer. After exposure for one year, the corrosion products were distributed randomly on the surfaces and might have formed initially on the active sites of the surface. The corrosion products were mainly composed of Al, O and Si. After exposure for 3 years, the corrosion products became dense and there was a high density of cracks. The corrosion products were composed of Al, O, Si, C and a trace amount of Cl and Ca according to EDS analysis. Elements (Si, Ca and Cl) are from the dust that was deposited on the surface of the 2A12-T3 alloy. The oxygen content increased with the exposure time, which indicated that the corrosion of the specimens became more severe.

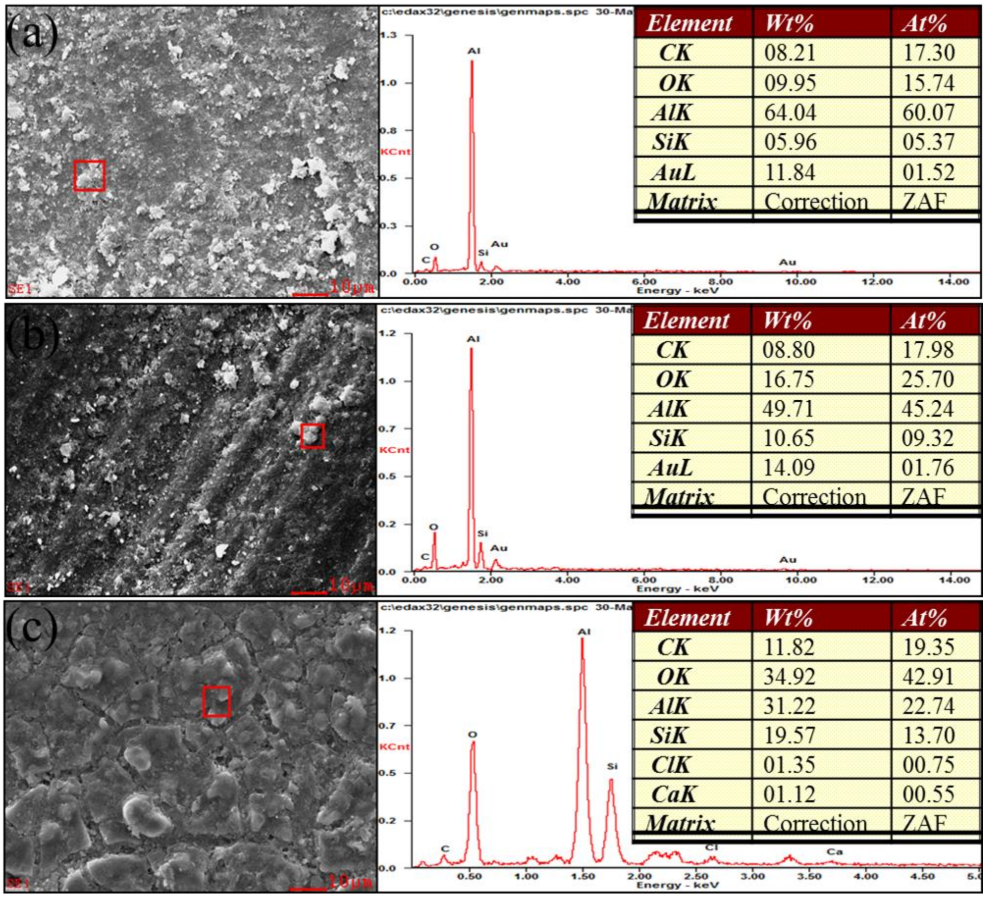

(a)

Element	Wt%	At%
CK	08.21	17.30
OK	09.95	15.74
AlK	64.04	60.07
SiK	05.96	05.37
AuL	11.84	01.52
Matrix	Correction	ZAF

(b)

Element	Wt%	At%
CK	08.80	17.98
OK	16.75	25.70
AlK	49.71	45.24
SiK	10.65	09.32
AuL	14.09	01.76
Matrix	Correction	ZAF

(c)

Element	Wt%	At%
CK	11.82	19.35
OK	34.92	42.91
AlK	31.22	22.74
SiK	19.57	13.70
ClK	01.35	00.75
CaK	01.12	00.55
Matrix	Correction	ZAF

Figure 7. SEM images and EDS spectra of the 2A12-T3 alloy after exposure in Turpan for(a) 1 year, (b) 2 years, and (c) 3 years.

The main compositions of the corrosion products that formed on the 2A12-T3 alloy specimens that were exposed at the Turpan test site for 1-3 years were analyzed by XRD and XPS techniques. Fig. 8 showed the X-ray diffraction patterns of the corrosion products from the specimens that were exposed for 1-3 years. The dominant corrosion products ($Al_2O_3 \cdot 4H_2O$, $Al(OH)_3$, AlOOH) were identified. In previous studies, the outer layer of the oxide film was reported to be porous and thick and mainly consisted of a hydrous form. The inner layer of the oxide film was thin and compact and mainly contained the aluminum oxide.

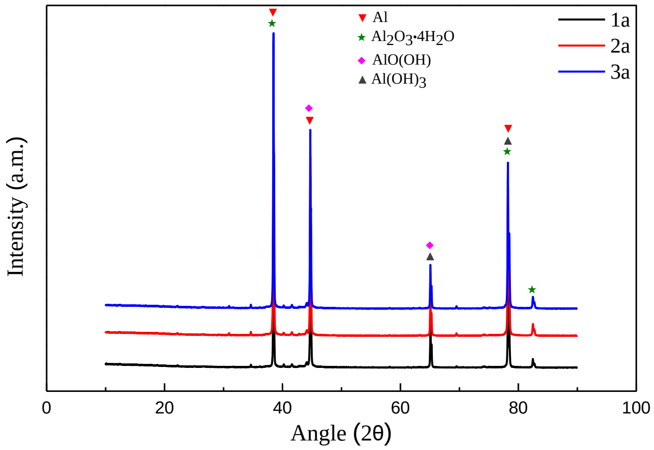

Figure 8. X-ray diffraction patterns after exposure at the Turpan test site for 1-3 years.

Fig. 9 shows the XPS spectra of the 2A12-T3 alloy specimens after exposure for 1-3 years in Turpan. Solid pollutants such as Cl, Si, and Ca were observed in the corrosion products in Fig. 9. The presence of these pollutants is attributed the high speed wind and occasional sand storms in Turpan. It's seen that spectra of Al 2p, O 1s and Cl 2p showed distinct peaks at approximately 74 eV, 531 eV, and 198.66 eV [18]. The XPS spectra for Al 2p and O 1s both displayed three peaks, as shown in Fig. 9 (b) and (c). The Al_2O_3 (73.90 eV) and $Al(OH)_3$ (74.80 eV) were detected as the main forms of the corrosion products, which is consistent with the results of XRD measurement. Additionally, the XPS results demonstrated that trace amounts of $AlCl_3$ (75.62 eV) were identified in the corrosion products. The Cl^- could penetrate into oxide film and lead to pitting due to its small ironic radius [19]. Consequently, the oxide films that formed on the 2A12-T3 alloy specimens in the Turpan generally were mainly comprised of Al_2O_3, bayerite ($Al(OH)_3$), boehmite (AlOOH) and $AlCl_3$.

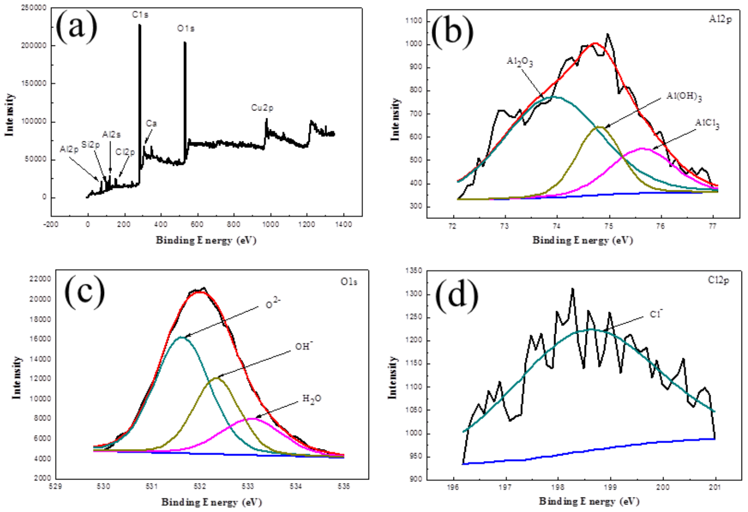

Figure 9. XPS analysis of the corrosion products that formed on the 2A12-T3 alloy after exposure in Turpan for 1-3 years.

3.4 Electrochemical impedance spectroscopy

Fig. 10 shows the EIS result for the 2A12-T3 alloy in 0.1% Na_2SO_4 solution after exposure in Turpan for 1-3 years. Fig. 10 (a) shows the Nyquist plots that were obtained for the 2A12-T3 alloy following various exposure times. The Nyquist plots of the specimens after exposure for 1 and 2 years at the Turpan test site exhibit a depressed semicircle from high to medium frequencies and an inductive loop at low frequencies, which could be related to the anodic dissolution during the initial stage when the samples were exposed to the aggressive environment. As shown in Fig. 10 (b), the Bode plots indicates that there exists at least two electrochemical process for the corrosion of 2A12-T3 alloy. According to previous literature [20, 21], the appearance of an inductive loop might be associated with pitting. Pits were observed to initiate most commonly around intermetallic particles, due to microgalvanic interactions between the intermetallic particles and the matrix [22]. Previous studies also found that pitting damage may trigger other forms of corrosion, such as intergranular corrosion [23] and stress corrosion cracking (SCC) [24]. The inductive loop was disappeared after exposure for 3 years, hence, the anodic process at the active sites stopped. Consequently, in the early exposure period, the pitting occurred on the surfaces of the 2A12-T3 alloy due to the presence of water droplets and galvanic interaction between intermetallic particles and the matrix. As the exposure time elapsed, the selective dissolution of active elements led to copper-rich remnants on the bottom of the pits. The corrosion rate in the vertical direction might be decreased or corrosion may terminate, In addition, dust particles were deposited on the surface of the 2A12-T3 alloy, which contained trace of chloride ions (in Fig. 4). The interaction between Cl- and Al_2O_3 produced the soluble chlorides, thereby resulting in the passive film breakdown. This might be the main reason for corrosion in the next stage.

The EIS spectra for various exposure times can be well-explained well by equivalent circuits as presented in Fig. 11. Fig.11 (a) is based on the Nyquist plots after exposure for 1 and 2 years and Fig. 11 (b) is based the Nyquist plots of specimens after exposure for 3 years. In the models, R_s was the solution resistance, R_{ct} was the charge transfer resistance and R_f was the constant phase element of corrosion product layer. The reciprocal of the charge transfer resistance (R_{ct}) was used as a constant to characterize the corrosion rate. The fitted results are listed in Table 4. The R_{ct} and R_f values of the 2A12-T3 alloy increased gradually with prolongation of exposure time, which was owing to the increase of the oxide film thickness. The corrosion products that formed on the surface of the 2A12-T3 alloy hindered the corrosion behavior to some extend. Hence, corrosion rate decreased as the exposure time extending.

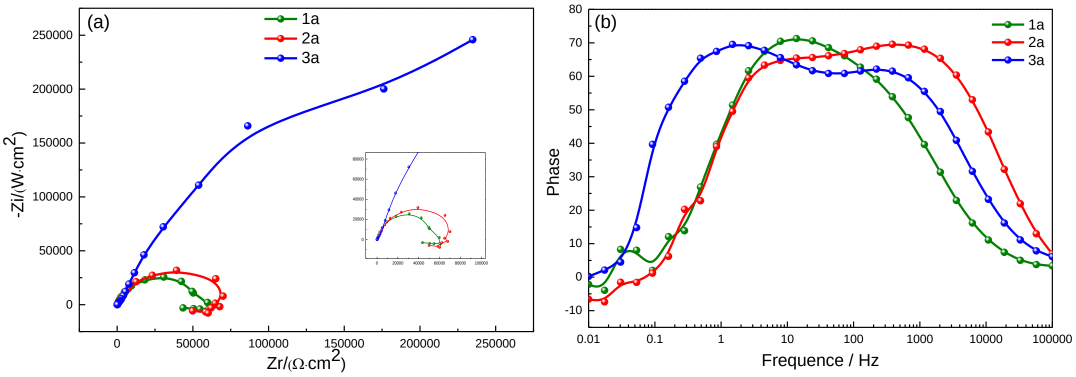

Figure 10. The EIS results for 2A12-T3 alloy specimens that were exposed in Turpan for 1-3 years: (a) the Nyquist plots (the figure in the right bottom is an enlargement of the Figure 10 (a)) and (b) the Bode phase plots.

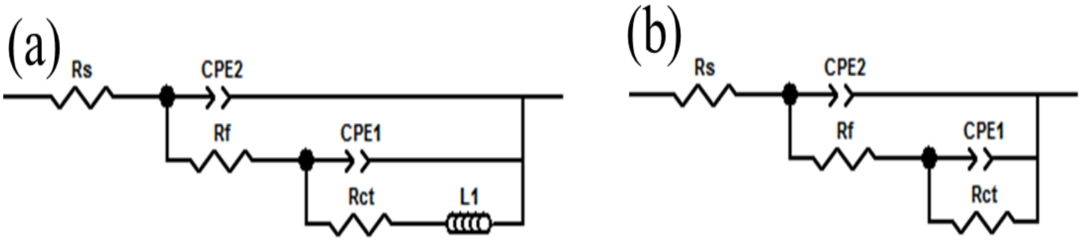

Figure 11. Equivalent circuit models proposed for the system in the experiment: (a) 1, 2 years; (b) 3 years

Table 4. The EIS fitting results that are base on the models that are shown in Figure 10 for the tested samples that were exposed to 0.1% Na_2SO_4 solution

T(a)	CPE_2(uF cm^{-2})	R_f(kΩ cm2)	CPE_1(uF cm^{-2})	R_{ct}(kΩ cm2)	X^2(10^{-3})
1	1.017	1.548	1.572	55.4	1.63
2	0.564	2.792	1.35	63.2	3.32
3	0.411	5.921	1.61	408.3	5.62

3.5 Surface potential difference

The corrosion behavior of the 2A12-T3 alloy was particularly influenced by the presence of the intermetallic particles due to their differing surface potentials with respect to the surrounding matrix [25-27]. Copper-containing intermetallic particles at the alloy surface were detrimental to the corrosion resistance because they provided preferential cathodic sites. The Al_2CuMg particle was the principle types of intermetallic particles that was crucial to the corrosion behavior in the 2A12-T3 alloy. The backscattered electron images of in Fig. 12 (a) show an Al_2CuMg particle, which was identified via EDS analysis in Fig. 12 (b).

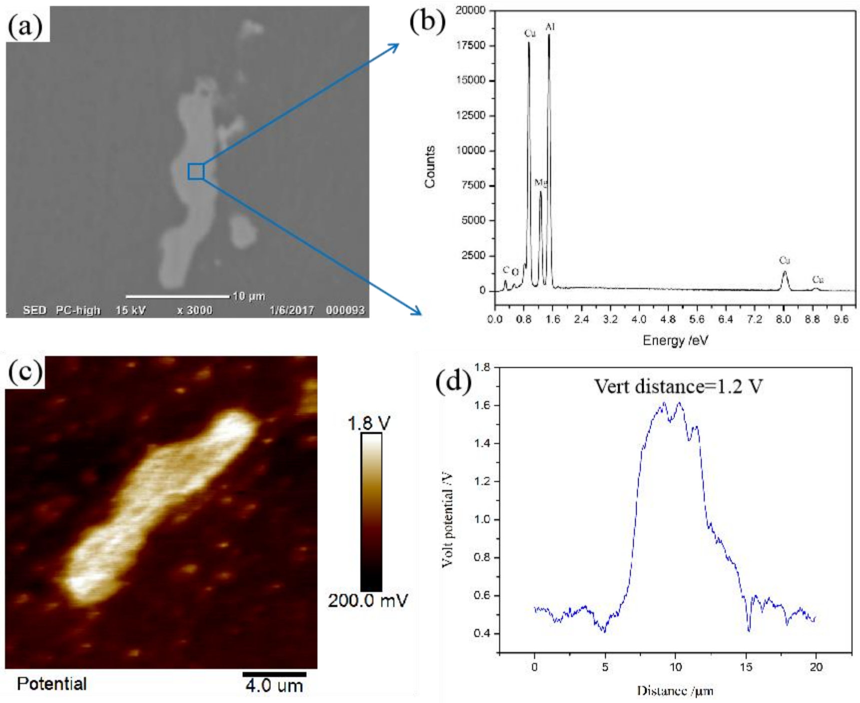

Figure 12. (a) An SEM image, (b) EDS spectrum, (c) Volta potential map and (d) section analysis of the Al_2CuMg phase in the 2A12-T3 alloy.

The size of the Al_2CuMg particles ranged between 4 µm and 10 µm. As shown in Fig. 12 (c) and (d), the surface potential of the Al_2CuMg particle was 1.2 V higher than that of the Al matrix, thereby demonstrating that the Al_2CuMg particle was noble than the surrounding Al matrix. Consequently, the

Al_2CuMg intermetallic particles, with the enrichment of copper acted as cathodic sites during the atmospheric corrosion behavior, while the surrounding Al matrix provided anodic sites. The metastable pitting was easily occurred on the surrounding Al matrix which had a lower surface potential. The dealloying of a less noble element might lead to the enrichment of the noble atoms on the bottom of pits. Thus, the pits propagated in a horizontal direction instead of propagation in the vertical direction. Hence, the size of the corrosion pits increased as exposure time extending as shown in Fig. 5.

3.6 Atmospheric corrosion behavior of the 2A12-T3 alloy at a dry-hot site

When the 2A12-T3 alloy was exposed to a tropical desert environment, an oxide layer formed on the surface, which was resistant to against corrosion. The oxide layer were consisted of Al_2O_3, bayerite ($Al(OH)_3$), boehmite (AlOOH) and a trace amount of $AlCl_3$. The corrosion mechanism of the 2A12-T3 alloy specimen that was exposed at the dry-hot site was mainly electrochemical corrosion, which consisted of the following cathode and anode reactions:

Anode reaction: $Al \rightarrow Al^{3+} + 3e^-$ (3)

Cathode reaction: $O_2 + 2H_2O + 4e^- \rightarrow 4OH^-$ (4)

In addition to the anode reaction to happen, the secondary reaction will also happen, resulting in the formation of inert alumina film [8], as illustrated in Equation (4) (5). From the thermodynamics point of view, it would improve the passivation performance of the aluminum alloy.

$$Al^{3+} + 3OH^- \rightarrow Al(OH)_3 \quad (5)$$

$$Al(OH)_3 \rightarrow AlOOH + H_2O \text{ or } Al(OH)_3 \rightarrow Al_2O_3 + H_2O \quad (6)$$

The film would be destructed by the aggressive species, such as chloride ions from the dust that were deposited on the surface of the 2A12-T3 alloy. According to the point defects model [28], Cl^- would replace O^{2-} in the oxide film to form soluble chloride, thereby resulting in thinning of the oxide layer by reaction/dissolution and directly attack of the substrate. However, the localized corrosion initially occurred on the interface of the intermetallic particles and Al matrix due to the galvanic reaction. In the dry and hot atmosphere, these corrosion rate was considerably lower than the corrosion rate in coastal, rural and industrial environment. With prolongation of the exposure time, the corrosion rate decreased due to increasing the thickness of the oxide film.

$$Al(OH)_3 + 3Cl^- \rightarrow AlCl_3 + 3OH^- \quad (7)$$

4. CONCLUSIONS

The corrosion behaviors of 2A12-T3 alloy specimens that were exposed at a dry-hot site for 1-3 years were investigated. The morphologies of the surface and cross-section were observed via SEM and optical microscopy. The compositions of the corrosion products were analyzed by EDS, XPS and XRD. The action mechanism of the corrosion products layer was investigated via EIS measurement. Four conclusions are summarized:

(1) The corrosion rates of the 2A12-T3 alloy in hot and dry atmosphere for 1-3 years were

respectively 0.62 $g\cdot m^{-2}\cdot a^{-1}$, 0.418 $g\cdot m^{-2}\cdot a^{-1}$ and 0.335 $g\cdot m^{-2}\cdot a^{-1}$, which can be described by the equation $C = 0.618t^{0.442}$. The average corrosion rate at the dry-hot site was considerably slower than the average corrosion rates in the coastal, urban and industrial atmosphere. With prolongation of the exposure time, the corrosion rate decreased.

(2) The surface corrosion products of the 2A12-T3 alloy specimens contained C, Al, O, Cl, Si, Cu and Ca elements in a dry tropical desert environment. The main component compounds of corrosion products were Al_2O_3, bayerite ($Al(OH)_3$), boehmite (AlOOH) and $AlCl_3$.

(3) The electrochemical behaviors of the 2A12-T3 alloy specimens that were exposed in Turpan for 1-3 years differed substantially. The specimens that were exposed for 3 years showed considerably higher corrosion resistance than the specimens that were exposed for 1 and 2 years. Therefore, the corrosion rate decreased with the exposure time extending.

(4) Pitting and intergranular corrosion were the main forms of the localized corrosion of the 2A12-T3 alloy. The initial damage was triggered by the microgalvanic corrosion due to the Volta potential difference between the intermetallic particles and the surrounding Al matrix.

ACKNOWLEDGEMENT

This work is supported by the National Key Research and Development Program of China (No. 2017YFB0702300) and the National Natural Science Foundation of China (No. 51671029). Supported by 111 Project (No. B170003).

References

1. Z.W. Qi, B. Q. Cong, B. J. Qi, G. Zhao and J. L. Ding, *Materials Letters*, 230 (2018) 275.
2. R. Rana, R. Purohit, S. Das, *International Journal of Scientific and Research Publications*, 2 (2012) 1.
3. Y. Liu, Y. Cheng, *Materials and corrosion*, 61 (2010) 211.
4. J. Li, N. Birbilis and R.G. Buchheit, *Corrosion Science* 101 (2015) 155
5. S.S. Z, *Corrosion Science*, 41 (1999) 1743.
6. D.D.L. Fuente, E.O. Huerta and M. Morcillo, *Corrosion Science*, 49 (2007) 3134.
7. S.Q. Sun, Q.F. Zheng, D.F. Li and J.G. Wen, *Corrosion Science*, 51 (2009) 719.
8. Z.Y. Zheng, T. Ma, W. Han and G.C. Yu, *Transactions of Nonferrous Metals Society of China*, l7 (2007) 326.
9. Y.D. Xiao, G.Y. Wang, X.G. Li, A. Lin, S.P. Zhang, X.Z. Qin, Z.Y. Wang, C.F. Liang, Q.F. Zheng and H.R. Mao, *Journal of Chinese Society for Corrosion and Protection*, 23 (2003) 248.
10. Z.Y. Wang, Q.X. Li, C. Wang, W. Han and G.C. Yu, *Transactions of Nonferrous Metals Society of China*, 17 (2007) 24.
11. Q.F. Zheng, S.Q. Sun, J.G. Wen and D.F. Li, *Transactions of Nonferrous Metals Society of China*, 19 (2009) 353.
12. D.D.L. Fuente, E.O. Huerta, M. Morcillo, *Corrosion Science*, 49 (2007) 3134.
13. S. Sun, Q.F. Zheng, D.F. Li and J.G. Wen, *Corrosion Science*, 51 (2009) 719.
14. B. B. Wang, Z.Y. Wang, W. Han and W. Ke, *Corrosion Science*, 59 (2012) 63.
15. C. Man, C.F Dong, Y.H. Fang, K. Xiao, C.Y. Guo, G. He and X.G. Li, *International Journal of*

Electrochemical Science, 10 (2015) 8691.
16. Z.Y. Cui, X.G. Li, K. Xiao and C.F. Dong, *Corrosion Science*, 76 (2013) 243.
17. Z.Y Cui, K. Xiao, C.F. Dong, Y. Ding, T. Wang and X.G. Li, *The Chinese Journal of Nonferrous Metals*, 23 (2013) 742.
18. T. Li, X.G. Li, C.F. Dong and Y.F. Cheng, *Journal of Materials Engineering and Performance*, 19 (2010) 591.
19. H.H. Strehblow and P. Marcus, *Corrosion mechanisms in theory and practice*, 8 (1995) 201.
20. S.Q. Sun, Q.F. Zheng, D.F. Li, J.G. Wen, *Corrosion Science*, 51 (2009) 719.
21. D.D.L. Fuente, E.O. Huerta and M. Morcillo, *Corrosion Science*, 49 (2007) 3134.
22. P. Leblanc and G. Frankel, *Journal of the Electrochemical Society*, 149 (2002) B239.
23. S. Jain, J. Hudson and J. Scully, *Electrochimica Acta*, 108 (2013) 253.
24. D. Najjar, T. Magnin and T. Warner, *Materials Science and Engineering:* A, 238 (1997) 293.
25. M.K. Cavanaugh, J.C. Li and N. Birbilis, *Journal of The Electrochemical Society*, 161 (2014) C535.
26. J.A. DeRose, T. Suter, A. Bałkowiec, J. Michalski, K.J. Kurzydlowski and P. Schmutz, *Corrosion Science*, 55 (2012) 313.
27. T. Hashimoto, X. Zhou, C. Luo, K. Kawano, G.E. Thompson, A.E. Hughes, P. Skeldon, P.J. Withers, T.J.Marrow and A.H. Sherry, *Scripta Materialia*, 63 (2010) 835.
28. D.D. Macdonald, *Electrochimica Acta*, 56 (2011) 1761.